Leg Design For Running and Jumping Dynamics

Daniel J. Blackman*, John V. Nicholson*, Jason L. Pusey†,
Max P. Austin*, Charles Young*, Jason M. Brown*, and Jonathan E. Clark*
*FAMU/FSU College of Engineering, Tallahassee, FL 32310
(djb14c, jn12c, mpa12c, cay03c, jmb10t)@my.fsu.edu, jeclark@fsu.edu
†U.S. Army Research Laboratory - Vehicle Technology Directorate
jason.l.pusey.civ@mail.mil

***Abstract*—Dynamic legged robots are capable of a wide range of behaviors, such as running, climbing, and jumping. Often the leg morphology and compliance are tailored to these specific behaviors. In this paper, we examine the design modifications to a 5-bar closed-loop kinematic leg design that enable both fast, stable running as well as energetic jumping. After investigating the running and jumping dynamics of the 5-bar leg design, control was implemented to transition between the desired configurations for each dynamic behavior in order to produce a desired maximum obstacle negotiation.**

I. Introduction

One of the advantages of legged mobility systems is the flexibility in the way in which the limbs can be used, depending on the environment. The same legs can be used to run, jump over obstacles, climb walls, and even swim [1]–[3]. The execution of each of these operations or tasks, such as jumping and running, however, has distinct dynamic requirements, and different combinations of leg design, stiffness, and control policy are required for peak performance. While these aspects are usually considered and optimized independently, this paper seeks to examine how they interact in combination to enable both dynamic tasks.

As a point of departure, we begin with the recently proposed planar, 2 DOF symmetric 5-bar[1] legs [5] utilized on Minitaur [6], [7]. This robot uses direct drive motors which result in high speeds and mechanical transparency. To compensate for the low torque of direct drive, large gap-radius motors and a symmetric 5-bar mechanism leg are employed. Experimental studies with this leg show that an unconventional configuration where the knee rides above the hip results in superior transduction of battery energy to body energy during jumping, yielding significantly higher jumps than a conventional design [5].

In contrast to hopping, primarily a 1D activity, running has typically been modeled using the planar, 2D Spring Loaded Inverted Pendulum (SLIP) Model [8] (Fig. 1a). This model accurately captures the ground reaction forces and center of mass motions for a wide scope of animals [9]–[12] and has also been applied toward the development and analysis of running gaits on robotic platforms [13]–[16], where the emphasis is usually on controlling the speed and ensuring the stability of the resulting gait. Previous works have shown

[1]The coaxial location of the motors at the hip is the main feature that distinguishes this is a 5-bar mechanism and affords the leg 2 DOFs (previously demonstrated with closed-loop manipulators [4]).

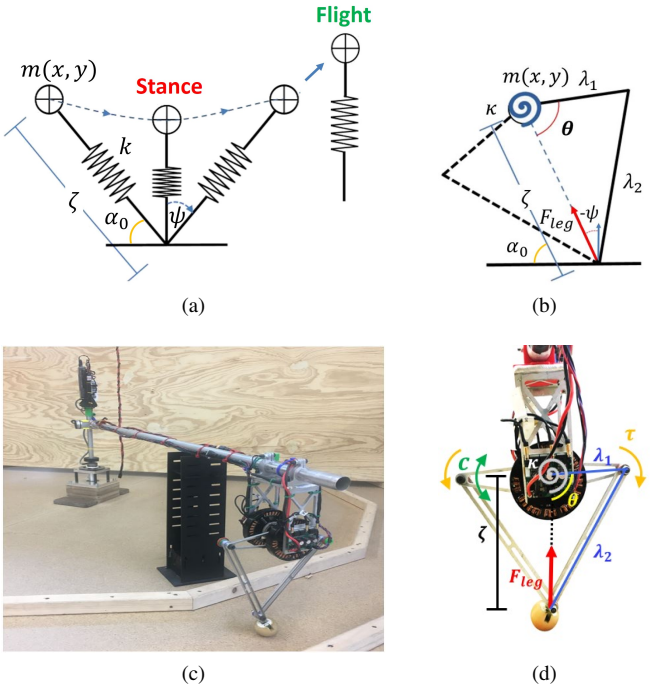

Fig. 1. The SLIP Model (a) is a standard method for modeling dynamic running. The system is defined by its parameters of mass (m), linear spring constant (k), leg length (ζ), and angle of contact (ψ). Translating these to a 5-bar leg system (b), the length (ζ) becomes a function of the angle of the hip (θ) with respect to the hip/toe axis and a torsional spring (κ) replaces the energetic return afforded via a linear spring. The experimental setup for this model (c) consists of a boom arm with a 5-bar leg attached at its end. The 5-bar leg (d) is shown with the characteristic parameters that describe its dynamic behavior.

that an articulated leg with an appropriate effective non-linear stiffness profile can improve the stability of running [17]–[19]. Jun et al. further showed that this effect diminishes as the leg link ratio departs from a 1/1 ratio [20].

In this paper, we utilize Minitaur's 5-bar mechanism as a tool to investigate the following questions:

- Does the non-conventional morphology that maximizes power transduction from the motor also improve the self-stabilizing behavior of the SLIP model?
- What are the effects of leg configuration and leg link length ratio on hop height and running stability?
- Can near-optimal running and jumping be achieved with

a single leg design?

Sections II and III introduce the simulations used to study the trade-offs between leg morphology and compliance for both running and jumping, featuring a 1D and a 2D SLIP-like model, both of which encode the 5-bar kinematics (see Fig. 1a, 1b). In section IV, the simulation is used to examine the relative importance of the leg design features. The results indicate that distinct postures are better for running and jumping, and switching kinematic configurations can enable the advantages of both of these desirable characteristics on the same platform. Sections V and VI describe how these results are then tested on a physical, one legged hopping robot for running and jumping (Fig. 1c, 1d) both individually and in a combined, dynamic action. Section VII summarizes these results and presents some possible directions for future work.

II. Simulation Models

For the 2D running studies, we modify the commonly used point-mass conservative SLIP model to include the kinematics of the 5-bar mechanism, as shown in Fig. 1b. The leg is considered massless and the foot is a frictionless pin joint during stance. For the hopping study, we analyze a 1D reduction of the SLIP model equipped with a motor model and constrained to operate in the vertical direction.

A. 5-bar SLIP Model

For the 5-bar SLIP model, the effective prismatic leg spring stiffness is defined by the torsional spring located at the hip, which can either be a physical or virtual (motor driven) spring, mitigated through the leg kinematics. Due to the symmetry of the system, the 5-bar mechanism can be simplified to a two-segment leg. Reminiscent of the work of Rummel & Seyfarth (2008), this leg can then be modeled utilizing a virtual leg setup with a realized nonlinear spring stiffness profile. The relationship between the leg force, F_{leg}, and the torque, τ, experienced at the hip will be used to calculate this relative nonlinear spring profile.

Similar to the derivations investigating two-segment legs with knee springs [17], the realization of this nonlinear spring stiffness in the spring-mass model is dependent on the hip angle, θ, as a function of the leg length, ζ:

$$\theta(\zeta) = cos^{-1}\left(\frac{\zeta^2 + \lambda_1^2 - \lambda_2^2}{2\lambda_1\zeta}\right) \tag{1}$$

With pre-determined link length values for the primary, λ_1, and secondary, λ_2, segments. Note, however, that the resulting relation is distinct from previous derivations since the torsional spring is located at the hip in this model.

Additionally, the nominal leg length, ζ_0, is defined by a given nominal hip angle, θ_0:

$$\zeta_0 = \sqrt{\lambda_2^2 - \lambda_1^2 + (\lambda_1 cos(\theta_0))^2} + \lambda_1 cos(\theta_0) \tag{2}$$

The nominal leg length and nominal hip angle define the unloaded, free position of the spring. To derive the equations of motion, substitution of the linear spring (standard to the SLIP model) with a torsional hip spring for the two-segment leg can be computed by replacement (i.e. instead of using $1/2k(\zeta_0 - \zeta)^2$, $1/2\kappa(\theta(\zeta_0) - \theta(\zeta))^2$ is used in the Lagrangian to incorporate the torsional spring dynamics). Using the Lagrangian method:

$$\frac{d}{dt}\left(\frac{dL}{d\dot{q}_i}\right) - \frac{dL}{dq_i} = 0 \tag{3}$$

where $q = [\zeta, \psi]$ for the stance phase of SLIP running. Thus, the equations of motion for stance are:

$$\ddot{\zeta} = \zeta\dot{\psi}^2 - gcos(\psi) + \frac{\kappa}{m}\frac{d\theta}{d\zeta}(\theta(\zeta_0) - \theta(\zeta)) \tag{4}$$

$$\ddot{\psi} = -\frac{2\dot{\zeta}\dot{\psi}}{\zeta} + \frac{g}{\zeta}sin(\psi) \tag{5}$$

where ζ is the dynamic leg length, ψ is the angle defined from the vertical center of the leg (parallel to the direction of gravity), g is the gravitational acceleration, κ is the torsional spring stiffness, and m is the point mass at the hip. The switching event (liftoff) occurs when the sum of the vertical components of the force are equal to zero and the hip has rotated past midstance ($\psi = 0$ when the hip is directly above the toe).

The flight phase of each stride is defined using projectile motion based on the final velocity produced from stance. The height of the center of mass (COM) at the designated touchdown angle marks the end of flight:

$$y_{TD} = \zeta_0 cos(\psi_{TD}) \tag{6}$$

where ψ_{TD} is the touchdown angle and is prescribed during the flight phase. No inertial effects impact motion during the flight phase where the legs are assumed to be massless. The parameters utilized for the model are based on a prototypical human runner [21], [22] and are listed in Table I.

TABLE I
Constant Parameter Values

Parameters	Human Values	Robot Values	Units
Mass (m)	80	1.45	(kg)
Spring Stiffness[a] ($\tilde{k}_{10\%}$)	$[1:50]$	$[8, 12.5, 16]$	N/a
Gravity (g)	9.81	9.81	(m/s^2)
Launch Height (y_{Apex})	1	≈0.3	(m)
Angle of Attack (α_0)	$[1:90]$	$[60:90]$	($degs$)
Input Velocity (v_x)	5	≈1.5	(m/s)
Segment Ratio[b] (R)	$[1/2, 1/1]$	$[1/2, 1/1]$	(m/m)
Nominal Hip Angle (θ_0)	$[0:90]$	$[75, 105]$	($degs$)
Nominal Length (ζ_0)	1	–	(m)
Segment 1 (λ_1)	Eq. 10	$[0.1, 0.1, 0.15]$	(m)
Segment 2 (λ_2)	λ_1/R	$[0.2, 0.1, 0.15]$	(m)

[a]Where $\tilde{k}_{10\%} = k_{10\%}\zeta_0/mg$
[b]Where $R = \lambda_1/\lambda_2$

B. 1D Hopper Simulation

For 1D hopping, the running model was modified to include an input torque. The input torque was defined using a standard motor model with parameters for the T-Motor U8 brushless DC motor used on Minitaur. [23]

$$\tau = \tau_{max} - \frac{\tau_{max}}{\omega_{NL}}\dot{\theta} \tag{7}$$

with a max torque, τ_{max}, of 7.66 Nm and no-load speed, ω_{NL}, of 168 rad/s (which are calculated form the motors velocity constant, K_v, and resistance, R_m provided [23]).

III. Conservative Simulation Study

Using the conservative SLIP model which instantiates the 5-bar leg kinematics (Eqs. 4-6), we investigate the relative effect of leg design, posture, and compliance on the stability of running.

A. Initial Model Setup and Conditions

1) Reference Stiffness for Comparison: The kinematics produce a non-linear stiffness profile through leg compression, necessitating the development of a referential stiffness for comparison. As is a common practice for analyzing human running, a reference stiffness is drawn between non-dimensional linear stiffness and the relative torsional spring stiffness at 10% compression, $\tilde{k}_{10\%}$ [17], [24]. This relation depends on the conversion between force and torque which is done using the virtual moment arm. This can be derived from the differential of Eq. 1,

$$\dot{\zeta} = \frac{d\zeta}{d\theta}\dot{\theta} \rightarrow F = \frac{d\theta}{d\zeta}\tau \tag{8}$$

From this expression, the torsional hip spring stiffness for a 10% compressed, two-segment leg can be calculated as:

$$\kappa = \tilde{k}_{10\%}\frac{mg}{\zeta_0}\frac{\Delta\zeta_{10\%}}{(\theta_0 - \theta_{10\%})}\frac{d\zeta}{d\theta} \tag{9}$$

where, $k_{10\%}$ is the relative linear spring stiffness, $\Delta\zeta_{10\%}$ is the length the leg is compressed ($0.1\zeta_0$), θ_0 is the nominal hip angle, $\theta_{10\%}$ is the hip angle at 10% length compression, and $d\zeta/d\theta$ is the Jacobian (8). For the purposes of comparison, this value is normalized to $\tilde{k}_{10\%} = k_{10\%}\zeta_0/mg$, providing a basis for comparison between different leg configurations.

2) Leg Length Normalization: Simulations were run on the basis of maintaining a constant nominal leg length through different hip angles and adjusting the segment lengths in order to accommodate the desired hip angle, nominal length, and ratio which can be solved algebraically using $R = \lambda_1/\lambda_2$ and Eq. 2 and solving for the segment lengths:

$$\lambda_1 = \frac{\zeta}{\sqrt{1/R^2 - sin(\theta)^2} + cos(\theta)} \tag{10}$$

3) Energy Input: For this study, we examine the effect of parameter variation on the range of leg touch down angles (the horizontal axes in Fig. 2) and we determine those gaits that converge to steady-state. This was done by setting an initial apex height of launch via the prescribed value, y_{Apex} in Table I (equivalent to the nominal leg length for the constant leg length and maximum leg length for constant segment length studies). The leg was launched from this apex with an initial velocity in the lateral direction (described as v_x in Table I).

4) Stability Analysis: After successfully completing 25 steps, a fixed point analysis of apex height perturbation was performed with a resolution of 10^{-6}m. This was done by running a single step of the successful gait and comparing it's output apex height to that of the same parameter set with initial perturbation. The diminishing deviation of the solution identifies it as steady state.

$$\left|\frac{d_{y_{i+1}}}{d_{y_i}}\right| < 1 \tag{11}$$

In which $d_{y_{i+1}}$ is the difference in the outputs between the perturbed and unperturbed step and d_{y_i} is the difference in the inputs (i.e. the perturbation).

IV. Simulation Results & Discussion

A. Ratio and Posture Effects on Running Stability

To visualize the effect of varying the link ratio (R) and touchdown configuration posture (θ) for the 5-bar leg with a torsional hip spring, Fig. 2 shows the stable range of touchdown angles for given non-dimensional stiffness values that produce stable running gaits. These plots include three different postures (an exaggerated knee below hip, $\theta = 45°$, knee below hip, $\theta = 75°$, and knee above hip, $\theta = 105°$) and variation of two different ratios between the primary and secondary links (maintaining symmetry of the mechanism).

Observing the results of the touchdown configuration posture, a few key features stand out. First, with adjusting the nominal configuration angle of the leg (θ_0) for either ratio, we observe that more upright configurations ($\theta_0 < 90°$) provide a slightly greater region of stability for SLIP-like running dynamics. A second observation is that the resultant torsional stiffness (secondary y-axis of each plot) required is generally lower for smaller configuration angles (i.e. longer leg lengths).

As leg link ratios deviate from $R = 1/1$ to $R = 1/2$ the size of the stable region of running slightly decreases, but these gaits also require significantly lower (a factor of $\approx$ 7-80 times!) torsional stiffness. This could arguably indicate that this design ($R = 1/2$) produces more efficient gaits since the proportional gain required of a motor is directly related to the torsional stiffness value.

The primary observation is that the region of stability, though similar, is only marginally smaller for $R = 1/2$. The torsional stiffness requirement (indicated in the second y-axis), however, is significantly impacted by configuration angle as well as link ratio. Thus it appears that the ideal set of parameters for running corresponds to the smallest configuration angle and lowest ratio value.

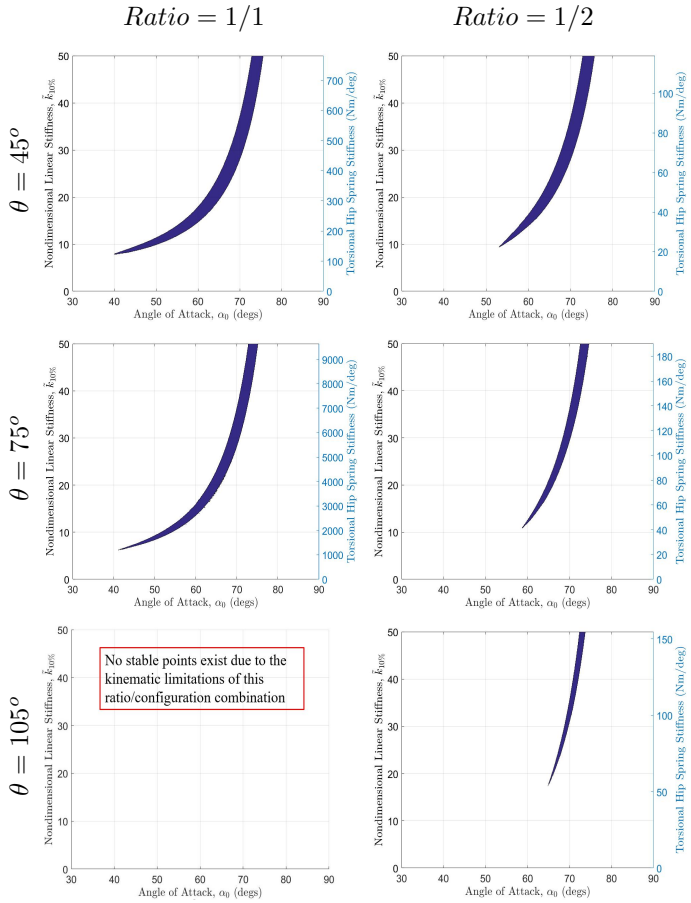

Fig. 2. Stability regions demonstrated here show the relative effects of ratio (columns) between the primary and secondary links and configuration posture (rows) on running stability of the 5-bar leg design. The axes are non-dimensional stiffness versus angle of attack ($\alpha_0 = 90 + \psi$), with a secondary y-axis on the right demonstrating the torsional stiffness constant of the resultant hip spring. The three posture angles (θ_0 = 45°, θ_0 = 75°, and θ_0 = 105°) were chosen based on the physical limitations of the robot (linkage collision occurs at angles less than $\theta = 45^o$) and previous work regarding knee springs and with a $R = 1/1$ ratio.

Finally, it is also noted that $R = 1/2$ affords the system the ability to run with an additional knee up posture, not attainable with the $R = 1/1$ leg. Figure 2 also shows an overlap of the knee up posture's stability region with each of the two knee down regions. This is key to work on incorporating maximum obstacle negotiation through the combination of fast, stable running and maximum hopping height (discussed later in Sections II-B, IV-B, & VI-C).

B. Hop Height Study

The model described in Section II-B was used to analyze the relative maximum achievable hop height as a function of leg link ratios with the given actuator voltage input. The maximum leg length of $\zeta_{max} = 0.3m$ was used to match the physical platform and provide resultant segment lengths of $\lambda_1 = R\zeta_{max}/(R+1)$ and $\lambda_2 = \lambda_1/R$. To maximize the resultant hop height, the full range of the configuration angle (θ) is swept for both the $R = 1/1$ and $R = 1/2$ linkage ratios. Additionally, a range of different effort levels (actuator input voltages) are swept to account for the other sources that will inevitably draw power from the system during steady state running in preparation for a running jump (i.e. maintaining the hip's rotational angle).

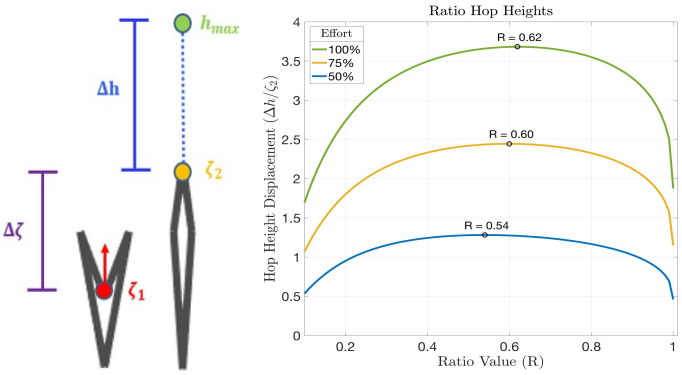

(a) (b)

Fig. 3. (a) The 1D hopping model performs a single jump, starting near full compression, extending until liftoff is achieved through force balancing between the actuator output and gravity. (b) For a range of different ratios at three designated control efforts (% voltage to motors), the hop height displacement demonstrated optimal ratios of 0.54, 0.60, and 0.62 (for 50%, 75%, and 100% effort, respectively).

Figure 3 shows the results of manipulating the ratio between the primary and secondary segments of the leg when the change in stroke length ($\Delta\zeta$) is maximized. From this simulation study, it is demonstrated that maximum hop heights are produced for $R = 0.54$ (50% effort), $R = 0.60$ (75% effort), and $R = 0.62$ (100% effort). For all levels of control effort, using a leg design with $R = 1/2$, yields jumps twice as high as $R = 1$ given this particular kinematic design and actuator.

V. Experimental Setup

In order to evaluate the veracity of the simulated results, an experimental platform was developed that allowed single leg hopping and running (see Fig. 1c). A single 5-bar leg was attached to the end of a $1.15m$ long aluminum boom arm in order to effectively restrict its motion to the sagittal-plane. The robot's touchdown point extends linearly off of the rear linkage of the robot and is covered by a 3D printed ABS plastic, spherical foot with an elastomeric covering to produce high friction between the ground and the effective leg which attempts to replicate point ground contact (reducing the effect produced by the toe extension present on the physical system). Contact events were registered from the leg via the motors' Hall Effect based, absolute encoders. To detect touchdown and liftoff, a force approximation is made based on the one dimensional Jacobian derived from the extension of the leg, ζ (Eq. 8). In order to track the robot's COM trajectory, Accucoder model 15s encoders, operating in the quadrature phase, are connected to the arm and base of the boom and produce resolutions of 0.14 mm and 0.044 mm respectively. This data was recorded using a National Instruments myRIO at 100 Hz

and compared to high speed video of each run in order to visually verify robot behavior.

The actuator transparency allows for proportional control to create a virtual spring which was experimentally tuned. The leg uses an event based controller which enforces passive rotation of the hip while the the leg is in stance and when the leg passes vertically below the center of mass, applies a constant torque. This torque value was 85% of the motors maximum value, allowing the other 15% to accommodate for the control of the virtual spring also produced by the motor. Upon liftoff, the robot resets to its original touchdown angle, preparatory for the next step.

VI. Experimental Results and Discussion

A. Running Experiments

In order to experimentally observe the simulated running trends obtained in Section IV-A, linkages were made at Minitaur's scale. These legs were made with a maximum length of $30cm$ resulting in link lengths of $\lambda_1 = 10cm$ and $\lambda_2 = 20cm$ for $R = 1/2$ (depicted in Fig. 1c & 1d) and $\lambda_1 = \lambda_2 = 15cm$ for a $R = 1/1$. Unfortunately, the $R = 1/1$ configuration ran into actuator limitations as predicted by simulation (Sec. IV-A) and could therefore not run. The $R = 1/2$ configuration, however, was run at three different postures; a knee up ($\theta = 105°$), knee down ($\theta = 75°$), and exaggerated knee down ($\theta = 45°$) configuration. Each of these configurations were then run at three non-dimensionalized relative leg stiffness values $\tilde{k}_{10\%} = [8, 12.5, 16.5]$ (defined in Table I and restricted by the motor limits of the physical system) over a prescribed range of touchdown angles. The stability of the robot is determined through the appearance of repeatable gaits, deemed to be successful if the leg makes more than three full revolutions of the track (total distance of $\approx 22m$) with observably steady state behavior.

TABLE II
Running Experimental Results

Nominal Hip Value (θ_0,°)	Spring Stiffness ($\tilde{k}_{10\%}$,-)	Lower Bound (α_0,°)	Upper Bound (α_0,°)	Range ($\Delta\alpha_0$,°)	Mean ($\overline{\alpha}_0$,°)
45 (Ex. Knee down)	16.5	66	70	4	68
	12.5	63.5	69	5.5	66.25
	8	60	68	8	64
75 (Knee down)	16.5	67	71.5	4.5	69.25
	12.5	65.5	70	4.5	67.75
	8	62.5	67	4.5	64.75
105 (Knee up)	16.5	69	70	1	69.5
	12.5	67.5	69	1.5	68.25
	8	64	65.5	1.5	64.75

From the data shown in Table II, it is evident that the same relative trends are observed on the physical system as previously seen in simulation. First, the width of the range of stable touchdown angles (see fifth column of Table II) is significantly greater (4°-8°) for exaggerated knee down and knee down configurations as opposed to knee up (1°-1.5°). Second, the trend of the stability region (demonstrated in the mean angle of Table II) follows a similar curve as the conservative simulation data with higher non-dimensional stiffness values resulting in steeper stable angles of attack. Finally, looking at the upper and lower boundaries outlined in the table, it is evident that there is generally overlap between configurations (i.e. $\theta = 45°$ and $\theta = 105°$), allowing for the smooth transition between any two provided they are set with a fixed touchdown angle that exists in both ranges.

B. Hopping Experiments

The simulation results described in Sec. IV-B suggest that linkage ratio can make a significant difference in maximizing hopping performance. To test this, the robot is constrained to a single dimension by holding the desired touchdown angle to be directly below the COM. Linkage sets with $R = 1/1$ and $R = 1/2$ were positioned at the same effective leg length during stance ($\zeta_1 = 0.11m$ to $\zeta_2 = 0.295m$[2] as depicted in Fig. 3a) and applied identical torque to both motors simultaneously to execute a full jump. In the $1/1$ case, link lengths $\lambda_1 = 15cm$ and $\lambda_2 = 15cm$ are used in order to ensure the same maximum leg extension during stance (Where $R = 1/2$ has link lengths $\lambda_1 = 10cm$ and $\lambda_2 = 20cm$). These jumps were run at 50%, 75%, and 100% of the motor effort (defined as the voltage supplied to the motor) for each leg. The jump height is averaged over 5 jumps and compared to the simulated results from Sec. IV-B and are plotted in Fig. 4.

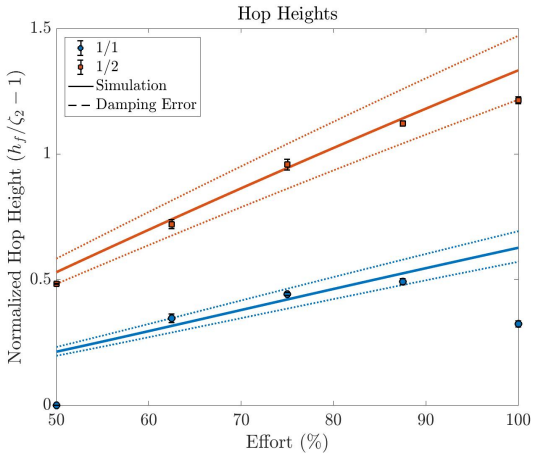

Fig. 4. Simulated hopping height with linkage ratios of $R = 1/1$ and $R = 1/2$ plotted with experimentally determined normalized COM hop height. This was evaluated over a range of values between 50% and 100% motor effort. In simulation, a linear damping constant (b) was determined using 75% effort and a range of $\pm 15\%$ of the determined value was swept for each respective ratio.

System losses such as motor inefficiency, the inertia of the boom, and joint viscosity could all attribute to the difference between the point data results and Figure 3. For this reason, the effect of this on either linkage configuration was simplified to a single linear damping value (b) and added to the simulation model, both in stance and flight:

[2]The physical limitations of the robot determine this range of values

$$\ddot{\zeta} = -g + \frac{\tau}{m}\frac{d\theta}{d\zeta} - \frac{b\dot{\zeta}}{m} \tag{12}$$

$$\ddot{y} = -g + b\dot{y} \tag{13}$$

The linear damping value (b) was obtained through running the *fsolve* Matlab function which use a LevenbergMarquardt algorithm for the simulation at 75% effort for each of the two separate linkage ratios to obtain the same maximum hop height[3]. The simulation was then run with this calculated damping value for each respective model over the span of effort levels (50-100%) with a tolerance of $\pm 15\%$, producing boundaries that generally encompass the experimental data. Exceptions exist for 50% and 100% effort for $R = 1/1$, however, which is postulated to be most likely caused by motor torque saturation and nonlinearity of the boom inertia.

C. Running and Hopping Experiments

Having established that the $R = 1/2$ leg can provide stable running and higher hopping, the next step involves combining these behaviors. From Sections IV-A and VI-A it was demonstrated that there exists overlap between the knee up and knee down postures' stability regions for the $R = 1/2$ linkage ratio. Additionally, Sections IV-B and VI-B demonstrated that this leg is nearly the most ideal for producing maximum hop heights given the particular actuator used.

To investigate the nature of combining these behaviors, parameters were determined based on the previous results for each individual behavior (Sections VI-A & VI-B). For running with the $R = 1/2$ linkage ratio, this included a knee down configuration ($\theta = 45°$) with an angle of attack $\alpha_0 = 68°$ and non-dimensional stiffness of 12.5 since this particular set of parameters produced the fastest gait at $\approx 2.6m/s$. For hopping with this ratio, the effort was increased to 100% and the length minimized to $11cm$ for the step preceding the obstacle. For $R = 1/1$, there was initially difficulty producing running gaits due to motor saturation since the torsional stiffness demands of this configuration were too large (as discussed in Sec. IV-A). For this reason, a smaller $R = 1/1$ leg was fabricated with linkage lengths of $\lambda_1 = \lambda_2 = 0.1m$. After an extensive parameter sweep, a single stable running gait was obtained with the following values: configuration posture of $\theta_0 = 22.5°$, angle of attack $\alpha_0 = 64°$, and non-dimensional stiffness of $\tilde{k}_{10\%} = 16.5$. These parameters produced a gait with speeds reaching $\approx 2.0m/s$. To account for the reduced nominal leg length of the $R = 1/1$ leg, the compress leg length prior to jump was reduced from $11cm$ to $7.33cm$ and the max effort was increased to 87.5% from 85%.

Figure 5 shows the normalized position of each of the robot with these linkage ratios approaching an obstacle of $\approx 2/3\ \zeta_2$ height. The $R = 1/1$ leg (top), even with smaller linkages

[3]At 75% effort, the simulation does not match with experimental data perfectly since the value is normalized to the liftoff length achieved which was observed to be a slightly different leg length across physical experiments and simulations

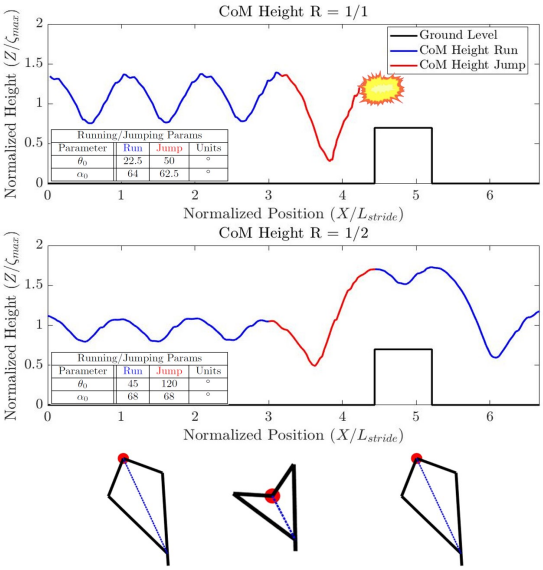

Fig. 5. Normalized COM hop height position showing $R = 1/1$ failing to clear the $2/3\ \zeta_2$ obstacle while the $R = 1/2$ ratio linkage leg successfully transitions between running and jumping gaits onto a $21cm$ platform. The parameters for both running and jumping are presented in the tables of each respective ratio's plot. Note that $\zeta_{max} = \lambda_1 + \lambda_2$ and L_{stride} represents the distance from peak to peak of steady state running. The bottom image depicts the leg configuration for running, the crouch in preparation for hopping, and the return to running posture.

to reduce the required motor output, is incapable of jumping the $13cm$ hop height (Δh) required to clear the obstacle. The $R = 1/2$ leg, however, clearly overcomes the obstacle and continues running after landing atop the $21cm$ block (Fig. 6).

VII. Conclusion and Future Directions

Simulation studies of the SLIP-like runner based on the symmetric 5-bar mechanism indicate that linkage design, posture, and spring stiffness all affect the stability of the system. Though decreasing the ratio between linkages has a marginal degradation effect on the stability region (region of fixed touchdown angles and stiffness values that produce stable running), the lower ratio requires much lower torsional values and allows the dynamic transition between a knee down and knee up configuration. The knee up configuration, as demonstrated previously, allows maximum hop height which was confirmed in simulation to be maximized by a ratio of $R = 0.54$-0.62 depending on available actuator energy. Experimental results confirmed the trends of changing stiffness and posture on running stability as well as maximizing hop height with the currently utilized $R = 1/2$ linkages. Understanding these key features and their effect on each of these dynamic motions enables us to combine these into a highly effective run-to-jump behavior.

The combination of fast, stable running of a $R = 1/2$ leg performing a squat-like jump to maximize hop height was successfully performed, achieving a height just over $2/3$ the maximum leg length. These experiments demonstrate that, per expectation, running with the knee down configuration affords

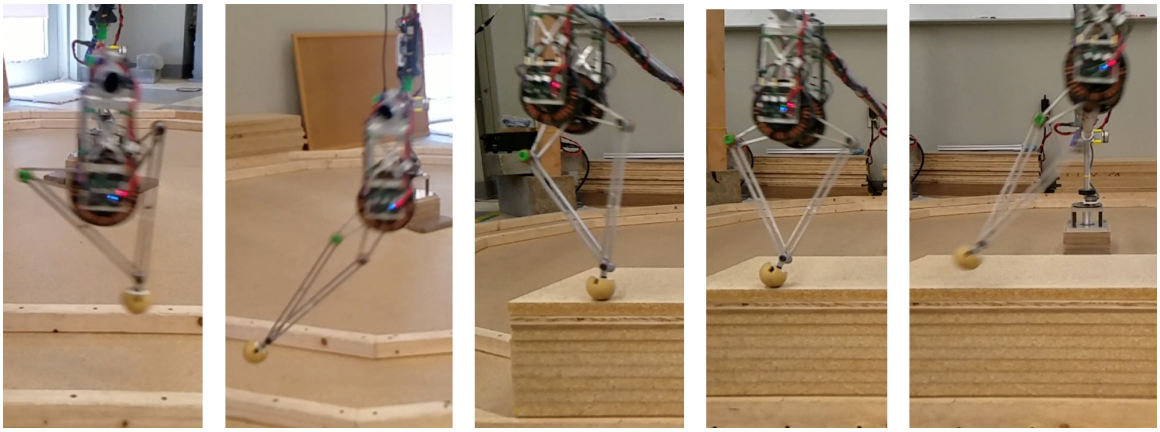

Fig. 6. From left to right: Robot compresses to a knee up configuration and performs a jump to land on the $21cm$ platform.

the system greater speed and stability and allows for the adjustment to the knee up configuration for improved obstacle negotiation.

Future work will explore the translation of these results to a quadruped running at steady state and jumping over obstacles, specifically analyzing running efficiency and obstacle negotiation in rough terrain environments.

ACKNOWLEDGMENTS

This work was supported by the collaborative participation in the Robotics Consortium sponsored by the U.S. Army Research Laboratory under the Collaborative Technology Alliance Program, Cooperative Agreement DAAD 19-01-2-0012, and by NSF Grant CMMI-1351524. The U.S. Government is authorized to reproduce and distribute reprints for Government purposes not withstanding any copyright notation thereon.

REFERENCES

[1] M. Raibert, M. Chepponis, and H. Brown, "Running on four legs as though they were one," *IEEE Journal on Robotics and Automation*, vol. 2, no. 2, pp. 70–82, Jun 1986.

[2] G. Dudek, M. Jenkin, C. Prahacs, A. Hogue, J. Sattar, P. Giguere, A. German, H. Liu, S. Saunderson, A. Ripsman *et al.*, "A visually guided swimming robot," in *2005 IEEE/RSJ International Conference on Intelligent Robots and Systems*. IEEE, 2005, pp. 3604–3609.

[3] B. D. Miller and J. E. Clark, "Towards highly-tuned mobility in multiple domains with a dynamical legged platform," *Bioinspiration & biomimetics*, vol. 10, no. 4, p. 046001, 2015.

[4] A. Bajpai and B. Roth, "Workspace and mobility of a closed-loop manipulator," *The International Journal of Robotics Research*, vol. 5, no. 2, pp. 131–142, 1986.

[5] G. Kenneally, A. De, and D. E. Koditschek, "Design principles for a family of direct-drive legged robots," *IEEE Robotics and Automation Letters*, vol. 1, no. 2, pp. 900–907, July 2016.

[6] D. J. Blackman, J. V. Nicholson, C. Ordonez, B. D. Miller, and J. E. Clark, "Gait development on minitaur, a direct drive quadrupedal robot," in *SPIE Defense+ Security*. International Society for Optics and Photonics, 2016, pp. 98 370I–98 370I.

[7] T. T. Topping, V. Vasilopoulos, A. De, and D. E. Koditschek, "Towards bipedal behavior on a quadrupedal platform using optimal control," in *SPIE Defense+ Security*. International Society for Optics and Photonics, 2016, pp. 98 370H–98 370H.

[8] R. Blickhan, "The spring-mass model for running and hopping," *Journal of biomechanics*, vol. 22, no. 11-12, pp. 1217–1227, 1989.

[9] C. T. Farley, J. Glasheen, and T. A. McMahon, "Running springs: speed and animal size," *Journal of experimental Biology*, vol. 185, no. 1, pp. 71–86, 1993.

[10] G. A. Cavagna, N. C. Heglund, and C. R. Taylor, "Mechanical work in terrestrial locomotion: two basic mechanisms for minimizing energy expenditure," *American Journal of Physiology-Regulatory, Integrative and Comparative Physiology*, vol. 233, no. 5, pp. R243–R261, 1977.

[11] R. Full and R. Blickhan, "Generality of spring-mass model in predicting the dynamics of many-legged, terrestrial locomotion," *Physiologist*, vol. 35, p. 185, 1992.

[12] N. C. Heglund, G. A. Cavagna, and C. R. Taylor, "Energetics and mechanics of terrestrial locomotion. iii. energy changes of the centre of mass as a function of speed and body size in birds and mammals," *Journal of Experimental Biology*, vol. 97, no. 1, pp. 41–56, 1982.

[13] R. Altendorfer, U. Saranli, H. Komsuoglu, D. Koditschek, H. B. Brown Jr, M. Buehler, N. Moore, D. McMordie, and R. Full, *Evidence for spring loaded inverted pendulum running in a hexapod robot*. Springer, 2001.

[14] B. Miller and J. E. Clark, "Towards highly-tuned mobility in multiple domains with a dynamical legged platform," *Bioinspiration & Biomimetics*, vol. 6, no. 2, p. 026009 (15), Jun 2015.

[15] S. Kim, J. E. Clark, and M. R. Cutkosky, "isprawl: Design and tuning for high-speed autonomous open-loop running," *The International Journal of Robotics Research*, vol. 25, no. 9, pp. 903–912, 2006.

[16] M. Hutter, C. D. Remy, M. A. Hopflinger, and R. Siegwart, "Slip running with an articulated robotic leg," in *Intelligent Robots and Systems (IROS), 2010 IEEE/RSJ International Conference on*. IEEE, 2010, pp. 4934–4939.

[17] J. Rummel and A. Seyfarth, "Stable running with segmented legs," *The International Journal of Robotics Research*, vol. 27, no. 8, pp. 919–934, 2008.

[18] J. D. Karssen and M. Wisse, "Running with improved disturbance rejection by using non-linear leg springs," *The International Journal of Robotics Research*, vol. 30, no. 13, pp. 1585–1595, 2011.

[19] M. S. Jones and J. W. Hurst, "Effects of leg configuration on running and walking robots," in *Proceedings of the 5th international conference on climbing and walking robots and the support technologies for mobile machines, Baltimore*, 2012, pp. 519–526.

[20] J. Y. Jun, D. Haldane, and J. E. Clark, "Compliant leg shape, reduced-order models and dynamic running," in *Experimental Robotics*. Springer, 2010, pp. 759–773.

[21] J. M. Schmitt, "Incorporating energy variations into controlled sagittal plane locomotion dynamics," in *ASME 2007 International Design Engineering Technical Conferences and Computers and Information in Engineering Conference*. American Society of Mechanical Engineers, 2007, pp. 1627–1635.

[22] A. Seyfarth, H. Geyer, and H. Herr, "Swing-leg retraction: a simple control model for stable running," *Journal of Experimental Biology*, vol. 206, no. 15, pp. 2547–2555, 2003.

[23] T-Motors, "U8 motor specifications," 2013.

[24] C. T. Farley and O. Gonzalez, "Leg stiffness and stride frequency in human running," *Journal of biomechanics*, vol. 29, no. 2, pp. 181–186, 1996.